

Photocatalytic Chemoselective C–C Bond Cleavage at Room Temperature in Dye-Sensitized Photoelectrochemical Cells

Shuya Li, Saerona Kim, Andrew H. Davis, Jingshun Zhuang, Eric Wolfgang Shuler, Debora Willinger, Jae-Joon Lee, Weiwei Zheng, Benjamin D. Sherman, Chang Geun Yoo, and Gyu Leem*



Cite This: *ACS Catal.* 2021, 11, 3771–3781



Read Online

ACCESS |



Metrics & More



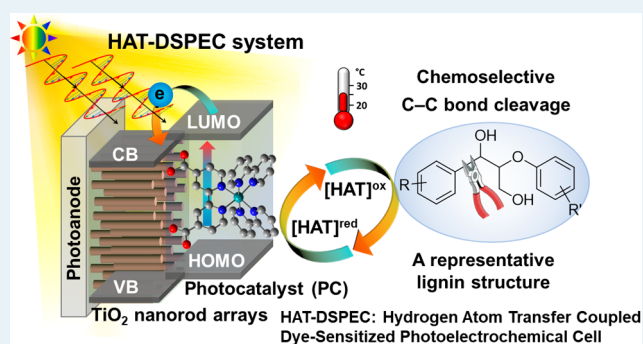
Article Recommendations



Supporting Information

ABSTRACT: Selective cleavage of C–C bonds can be a valuable tool for various applications including polymer degradation and biomass utilization. Performing chemical transformations involving C–C bond cleavage steps under mild conditions and ambient temperature remains challenging due to the high dissociation energies of the C–C bond. This fundamental challenge can be solved by coupling a dye-sensitized photoelectrochemical cell (DSPEC) system, that generally targets the water splitting reaction, with a hydrogen atom transfer (HAT) mediator (HAT-DSPEC). Here, we report the solar-driven selective cleavage of the C(aryl)–C(alkyl) σ -bond in lignin at ambient temperature using an HAT-DSPEC under redox-neutral conditions. The photocatalyst (bis-2,2'-bipyridine)(2,2'-bipyridine-4,4'-dicarboxylic acid)Ru(II) (**RuC**) adsorbed onto a TiO₂ nanorod array with the length of $\sim 1.6 \mu\text{m}$ and a rod diameter of 100 nm atop fluorine-doped tin oxide (FTO/TiO₂ NRAs/RuC) film was prepared and investigated with an HAT mediator, 4-acetamido 2,2,6,6-tetramethylpiperidine-1-oxyl (ACT), in solution. Photophysical and electrochemical studies of **RuC** and ACT with a lignin model compound, 1-(4-hydroxy-3,5-dimethoxyphenyl)-2-(2-methoxyphenoxy) propane-1,3-diol (**LMC**) reveal that the metal-to-ligand charge transfer (MLCT) excited states from the **RuC** are efficiently quenched in the presence of ACT with **LMC**. The HAT-DSPEC photoanode, containing the surface-bound photocatalyst **RuC** at the photoanode with ACT and **LMC** in solution, sustained an excellent photocurrent density, significantly outperforming that with the photocatalyst **RuC** alone. Moreover, the chemoselective cleavage of the C(aryl)–C(alkyl) bond in the **LMC** at the ambient temperature was demonstrated in the HAT-DSPEC system with a remarkable photocatalytic turnover number (>3000) leading to excellent selectivity ($>90\%$) of C–C bond cleavage under AM1.5G irradiation (1 sun, 100 mW cm^{-2}). These results were obtained over short reaction times and mild, redox-neutral reaction conditions without the need for extended reaction time (e.g., $>24 \text{ h}$) or high temperature that is typical of homogeneous catalytic systems. This is the first report to demonstrate that an HAT-DSPEC can serve as a viable method for performing visible-light-driven selective C–C bond cleavage at ambient temperature.

KEYWORDS: heterogeneous photocatalysis, bond cleavage, solar energy, lignin, dye-sensitized photoelectrochemical cell, hydrogen atom transfer



INTRODUCTION

Selective cleavage of C–C bonds is a useful chemical transformation in organic synthesis and the chemical industry.^{1–3} This transformation is integral for the depolymerization of lignin, a sustainable and renewable feedstock.^{1,4–6} Lignin is the largest noncarbohydrate component in lignocellulosic biomass and features aromatic functional groups distributed within a highly branched macromolecule structure, covalently linked by aliphatic ether bonds.⁷ The carbohydrate and/or aromatic-rich fraction is converted to biofuel through fermentation.^{8–10} Thus, the conversion of lignin into valuable low-molecular-weight chemicals has been considered as a marketable application in the pulping and paper industry.^{11–13} It also represents a renewable alternative to petroleum as a

source for the production of low-molecular-weight aromatic chemicals (e.g., catechol) that serve as feedstocks for the chemical industry.¹⁴ Recent research for lignin valorization is focused on chemical strategies for depolymerization affording high selectivity and productivity under mild reaction conditions, to enable the formation of well-defined and targeted aromatic chemical building blocks. Several electro-

Received: January 14, 2021

Revised: February 27, 2021

Published: March 11, 2021



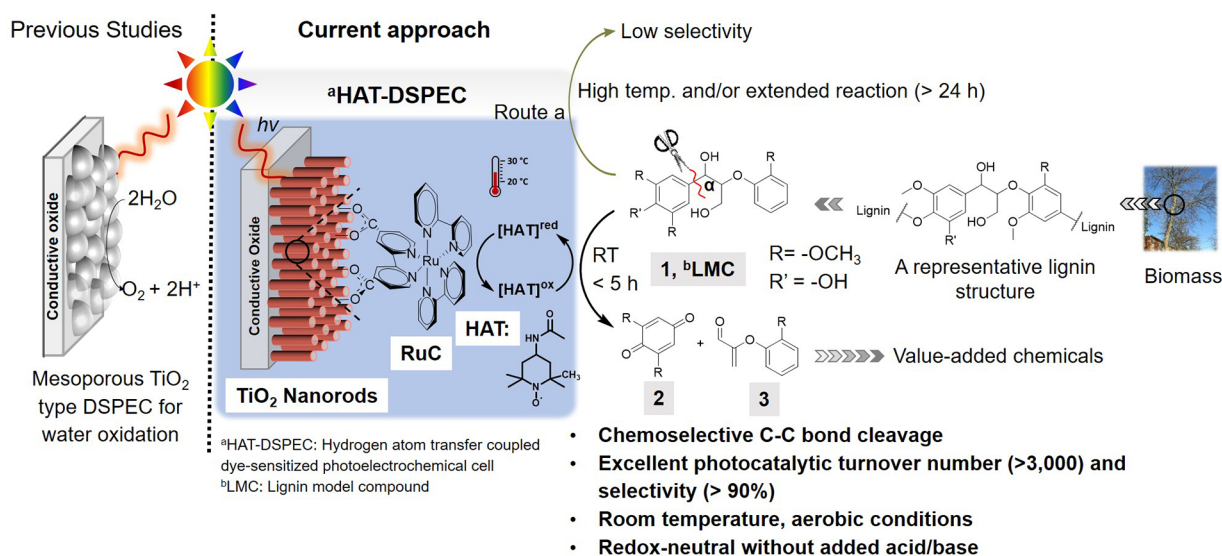


Figure 1. Illustration of a mesoporous structured TiO₂ type DSPEC containing a Ru-based chromophore–water oxidation catalyst assembly system for solar-driven water oxidation (previous studies) and a one-dimensional TiO₂ nanorod type dye-sensitized photoelectrochemical cell incorporated with a hydrogen atom transfer mediator (HAT-DSPEC, current approach). The TiO₂ nanorods (TiO₂ NRAs) grown on fluorine-doped tin oxide (FTO) glass substrate (FTO|TiO₂ NRAs) followed by the immobilization of photocatalyst RuC were used as the photoanode. The HAT-DSPEC is a single compartment three-electrode cell with the photoanode, platinum wire, and nonaqueous Ag/Ag⁺ electrode incorporated with the soluble hydrogen atom transfer mediator in nonaqueous solvent. The β-aryl ether linkage containing a phenolic group is shown in a representative lignin fragment. In the conventional route a, C_{aryl}–C_α bond cleavage proceeds under high temperature and/or extended reaction time using a homogeneous metal catalyst.

chemical and photochemical reactions have been performed for lignin depolymerization that proceed under mild conditions.^{15–20} For example, the Stephenson group has reported a highly selective two-step (alcohol oxidation followed by reductive cleavage) depolymerization of native lignin at ambient temperature via electrochemical and photochemical approaches under mild conditions.¹⁶ In 2020, we reported a photochemical system for the initial oxidation of the secondary benzylic alcohols in lignin model compounds and real lignin as part of a selective two-step process prior to C–O bond cleavage in the lignin backbone.²¹

Environmentally sustainable and renewable energy technologies require more widespread use of solar energy. Dye-sensitized photoelectrochemical cells (DSPECs) offer a method of using renewable solar energy to drive energetically demanding chemical conversions.^{22,23} Meyer, Schanze, and co-workers have developed a DSPEC for solar-driven water oxidation or hydrogen production for the generation of solar fuels.^{22,24–27} DSPECs utilize n- or p-type mesoporous structured semiconductor oxides with surface-bound molecular chromophore–catalyst assemblies to carry out water oxidation or water/proton reduction. Though significant progress has been made in the past decade, light-driven water splitting remains a major challenge because of the short-term stability of molecular light-harvesting materials and the thermodynamic and/or kinetic barriers for the required chemical reactions in aqueous media under solar light illumination.²⁸ Thus, in light of the challenges facing DSPECs for solar fuels, our previous study explored applying a conventional mesoporous TiO₂ type DSPEC with a hydrogen atom transfer (HAT) mediator in the presence of a base in nonaqueous media for selective oxidation of 2° benzyl alcohol moieties in lignins.²¹ This approach requires a second step to complete the C–O/C–C bond cleavage with additional photosensitizers. Moreover, the C–C bonds cannot be fully oxidized electrochemically or photo-

chemically at room temperature.²⁹ Specifically, examples of the direct bond cleavage of C_{aryl}–C_α at room temperature are rare and require elevated temperature (e.g., 80 °C) and/or extended reaction periods (>40 h), and the presence of a catalyst.^{30,31} However, despite this progress, no heterogeneous photocatalytic systems for the cleavage of the aryl α-carbon bond in lignin substrates have been reported using a DSPEC system at ambient temperature without the need of base or acid.

This report presents a heterogeneous photocatalytic process to cleave the C_{aryl}–C_α bond in a phenolic lignin model compound using a one-dimensional TiO₂ nanorod array type DSPEC coupled with a HAT mediator (HAT-DSPEC, Figure 1). This system operates under solar light irradiation, at ambient temperature, and in an open-air environment without the need of additional base or acid. Previously, mesoporous surfaces prepared from TiO₂ nanosphere sol–gels are most commonly used for dye-sensitized photoanode (Figure 1, previous studies);³² however, TiO₂ nanorod array electrodes were selected for this study because the one-dimensional morphology with a high aspect ratio of the crystalline TiO₂ nanorod arrays (TiO₂ NRAs) can facilitate charge transport through a direct electrical path to the conductive fluorine-doped tin oxide (FTO) surface.³³ The HAT-DSPEC incorporates TiO₂ nanorod arrays on FTO (FTO|TiO₂ NRAs), a polypyridyl Ru photocatalyst containing dicarboxylic acid anchoring groups [RuC, (bis-2,2'-bipyridine)(2,2'-bipyridine-4,4'-dicarboxylic acid)Ru(II)], and 4-acetamido-2,2,6,6-tetramethyl-1-piperidine-N-oxyl (ACT) as an HAT mediator. Polypyridyl Ru(II) complexes have been extensively used as light-harvesting units for dye-sensitized solar cells, in artificial photosynthesis for solar fuels, as well as for in vitro cellular and in vivo applications due to their excellent photophysical properties such as long excited-state lifetimes and high absorptivity in the visible spectrum from a strong metal-to-

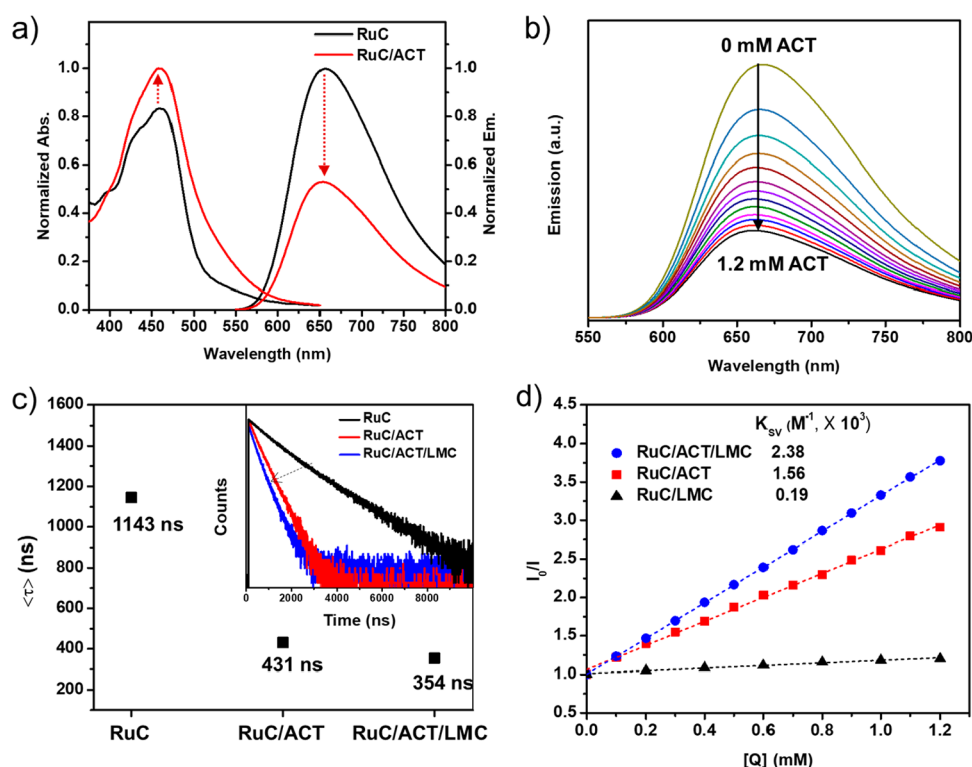


Figure 2. (a) Absorption and emission spectra of RuC (black lines) and RuC/ACT (red lines) in acetonitrile (ACN). Absorption and emission spectra were normalized to the λ_{\max} value. Emission spectra were acquired with excitation at $\lambda_{\text{ex}} = 410$ nm. (b) Emission quenching for RuC with ACT ($c = 0\text{--}1.2$ mM) in ACN solution. (c) Comparison of emission lifetimes of RuC, with ACT and both ACT and LMC in solution. (Inset: the time-resolved emission traces are shown.) (d) Stern–Volmer plots (I_0/I vs $[Q]$, Q: ACT, LMC, or ACT and LMC) for emission quenching of RuC with LMC (black triangle), ACT (red square), and both ACT and LMC (blue dots) by monitoring the emission intensity at 667 nm ($\lambda_{\text{ex}} = 410$ nm).

ligand charge transfer (MLCT) transition.^{34–38} ACT, an organic nitroxyl radical, is used as the mediator for oxidation of benzylic alcohol functional groups in lignin due to its high nitroxyl/oxoammonium redox potential and chemical stability.²⁰ Figure 1 represents the chemoselective $C_{\text{aryl}}\text{--}C_{\alpha}$ bond cleavage in a β -aryl ether dimeric lignin model compound (LMC) by the HAT-DSPEC with solar light illumination at ambient temperature under redox-neutral conditions. This LMC structure containing the most abundant interunit linkage in native lignin is used as a representative lignin model compound.

RESULTS AND DISCUSSION

The initial study focused on examining the photophysical properties of RuC with ACT in acetonitrile (ACN) solution and at the interface of an FTO/TiO₂ NRAs electrode. The UV–vis absorption and photoluminescence emission spectra of RuC indicate a strong MLCT absorption band with $\lambda_{\max} \sim 460$ nm and a distinguished emission with $\lambda_{\max} \sim 656$ nm arising from the ³MLCT excited state (black solid lines) in Figure 2a. ACT displays a similar absorption band with $\lambda_{\max} \sim 460$ nm and an overlapped emission band with $\lambda_{\max} \sim 646$ nm in Figure S1. After the addition of ACT to the RuC solution, the absorption near 460 nm slightly increases due to the additive contribution of ACT in this spectral range; however, the emission intensity from the excited-state RuC* decreases substantially in the presence of ACT (red solid line in Figure 2a). This observation suggests efficient charge transfer from photoexcited RuC* to ACT. To demonstrate the effect of ACT on the RuC* emission, quenching and fluorescence

lifetime measurements were carried out in the presence of an increasing concentration of ACT (ranging from 0 to 1.2 mM) in ACN solution at room temperature. Figure 2b shows that emission from RuC* was efficiently quenched by the presence of ACT revealing a Stern–Volmer quenching constant value (K_{sv}) $\sim 1.56 \times 10^3 \text{ M}^{-1}$. The Stern–Volmer plot for emission quenching of RuC with ACT is shown in Figure 2d. Our previous work has demonstrated the quenching of RuC in the presence of both hydrogen transfer agent *N*-hydroxyphthalimide (NHPI), a related nitroxyl HAT species, and the base 2,6-lutidine.²¹ It is interesting to note that the quenching of RuC* emission with ACT shows a ~ 3 -fold amplification in quenching efficiency without the need for a base compared to that of the NHPI/base pair. This enhanced quenching effect of ACT with photoexcited RuC* can lead to an excellent photocatalytic performance in the HAT-DSPEC system under visible light illumination. Moreover, as shown in Figure 2c, the average emission lifetimes for RuC* in the absence and presence of ACT were 1143 and 431 ns, respectively, in ACN solution. The emission lifetime of RuC* in the presence of ACT decreased significantly which is consistent with the above quenching experiments. These observations present strong evidence for electron transfer between photoexcited RuC* and ACT under visible light illumination, resulting in the formation of RuC(III) or/and oxidized ACT.

Encouraged by these results, we next investigated the photophysical properties of RuC and ACT (RuC/ACT) in the presence of the LMC. Upon the addition of LMC, the emission lifetime of the RuC/ACT decreases from 431 to 354 ns as shown in Figure 2c. The observed behavior can be

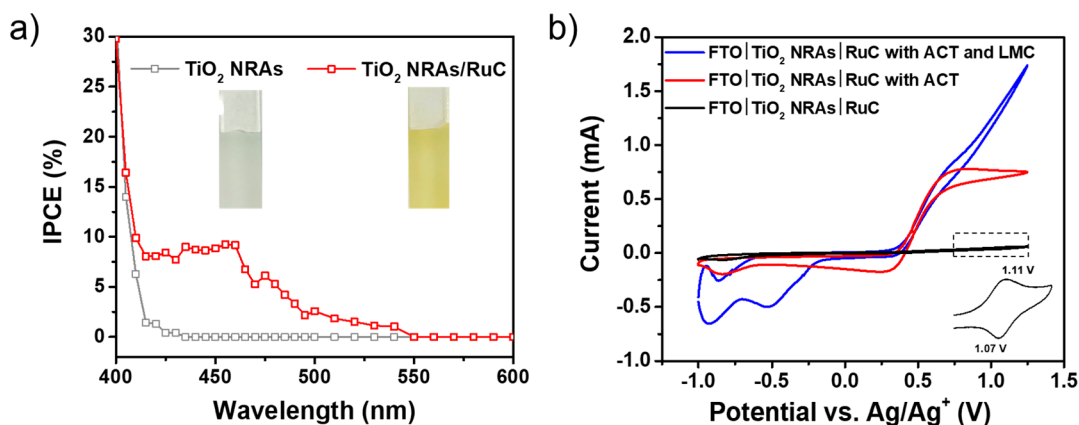


Figure 3. (a) Incident photon to charge carrier efficiency (IPCE) tests for an FTO/TiO₂ NRAs electrode (gray dots) and TiO₂ NRAs coated with RuC (FTO/TiO₂ NRAs/RuC) (red dots). The pictures of FTO/TiO₂ NRAs electrodes without and with RuC are shown in the inset. (b) CVs of FTO/TiO₂ NRAs/RuC (black), the same with 3 mM ACT (red), and both 3 mM ACT and 8 mM LMC (blue).

explained by the intermolecular energy/electron transfer process between RuC/ACT and LMC that can drive photocatalytic oxidation of LMC under visible light illumination. Figure 2d illustrates the Stern–Volmer plots and lists the K_{sv} of RuC/LMC, RuC/ACT, and RuC/ACT/LMC. On the basis of the lifetime measurement above, the persistence of RuC* was largely unaffected by the presence of LMC in the absence of ACT. Increasing the concentration of LMC from 0 to 1.2 mM in the RuC acetonitrile solution, with no ACT present, showed slight quenching with $K_{sv} \sim 0.19 \times 10^3 \text{ M}^{-1}$. The Stern–Volmer constants were calculated according to eq 1 where I_0 is the initial emission intensity of the RuC solution, I is the emission intensity of RuC in the presence of Q (Q = ACT, LMC, or ACT and LMC), and [Q] is the quencher concentration. The steady-state emission spectra of RuC with increasing ACT/LMC pair concentrations ($c = 0\text{--}1.2 \text{ mM}$ in ACN solution) are shown in Figure S2. Consistent with the emission lifetime measurements above, RuC was efficiently quenched by the ACT/LMC pair, revealing a $K_{sv} \sim 2.38 \times 10^3 \text{ M}^{-1}$, in comparison to the quenching of RuC/ACT without LMC ($K_{sv} \sim 1.56 \times 10^3 \text{ M}^{-1}$). From these results, it is concluded that the presence of LMC regenerates ACT from oxoammonium ACT⁺ formed following the photoexcited energy/electron transfer between RuC(II)* and/or RuC(III) and ACT.

$$\frac{I_0}{I} = 1 + K_{sv}[Q] \quad (1)$$

Observation of enhanced RuC* emission quenching in the presence of ACT and LMC in solution indicated the viability of developing a heterogeneous HAT-DSPEC system with the overall goal of facilitating light-driven oxidative C_{aryl}–C_α bond cleavage in lignin at ambient temperature. The FTO/TiO₂ NRAs films were prepared by a hydrothermal reaction and annealed at 400 °C for 3 h according to the previous study.^{39,40} The top-down and cross-sectional morphologies of FTO/TiO₂ NRAs were characterized by scanning electron microscopy (SEM) (Figure S3). The TiO₂ NRAs are perpendicular to the surface of the FTO substrate. The corresponding average diameter and length of the TiO₂ nanorods were approximately 100 nm and 1.6 μm, respectively. The thickness of the TiO₂ NRAs by SEM is consistent with the film height, 1.5 μm, measured by profilometry (data not shown here). In Figure 1, RuC is shown covalently immobilized onto the FTO/TiO₂

NRAs' surface by the interaction of the polar carboxylate moieties of RuC (FTO/TiO₂ NRAs/RuC). RuC was adsorbed onto an FTO/TiO₂ NRAs semiconductor electrode (1.16 mM RuC in acetonitrile solution for 12 h) as previously reported.^{37,41} The MLCT absorption and steady-state emission of FTO/TiO₂ NRAs/RuC film corresponded to a blue-shifted absorption and emission bands with $\lambda_{max} \sim 454$ and 643 nm, respectively, compared to that of RuC in ACN solution (Figure S4). The surface coverage of RuC on the TiO₂ NRAs was quantified by calculating the molar surface concentration of RuC according to the previous equation.⁴² The calculated surface coverage for RuC onto the TiO₂ NRA film with a thickness of $\sim 1.6 \mu\text{m}$ was $\sim 5.29 \times 10^{-9} \text{ mol cm}^{-2}$ (Table S1). This surface coverage is consistent with that of polymer-based Ru(II) chromophores containing carboxylic acid moieties on mesoporous TiO₂ film from our previous study.⁴¹

To demonstrate electron injection of photoexcited RuC* into one-dimensional TiO₂ NRAs, incident photon-to-current efficiency (IPCE) measurements were conducted with the FTO/TiO₂ NRAs electrode before and after the immobilization of RuC as shown in Figure 3a. The IPCE spectrum showed a maximum value of $\sim 10\%$ at $\sim 460 \text{ nm}$ that corresponds to the MLCT absorption band maximum of the RuC in an FTO/TiO₂ NRAs/RuC film, while a bare FTO/TiO₂ NRAs substrate did not show photocurrent in the visible spectrum. Cyclic voltammetry (CV) was carried out in acetonitrile solution containing 0.1 M tetrabutylammonium hexafluorophosphate (TBAPF₆) to study the electrochemical response of the FTO/TiO₂ NRAs/RuC surface in the dark in the presence or absence of ACT and LMC with representative voltammograms shown in Figure 3b. The FTO/TiO₂ NRAs/RuC in a neat electrolyte (black voltammogram in Figure 3b) shows a characteristic redox couple for the surface-bound RuC^{III/II} with $E_{1/2} = 1.09 \text{ V}$ vs Ag/Ag⁺ (Figure 3b, inset). Introduction of ACT to the solution (red voltammogram in Figure 3b) brought on a new wave with a more cathodic onset compared to the RuC^{III/II} couple beginning around 0.3 V vs Ag/Ag⁺. This wave shows diffusional character, and the steady-state current at potentials $>0.7 \text{ V}$ vs Ag/Ag⁺ is dependent on the concentration of ACT added to the solution. This wave is attributed to the oxidation of ACT to the oxoammonium species ACT⁺. A similar wave is observed with an FTO/TiO₂ NRAs surface (no bound RuC), and therefore, RuC is not implicated in mediating this process (Figure S5). This result does indicate that applied biases higher

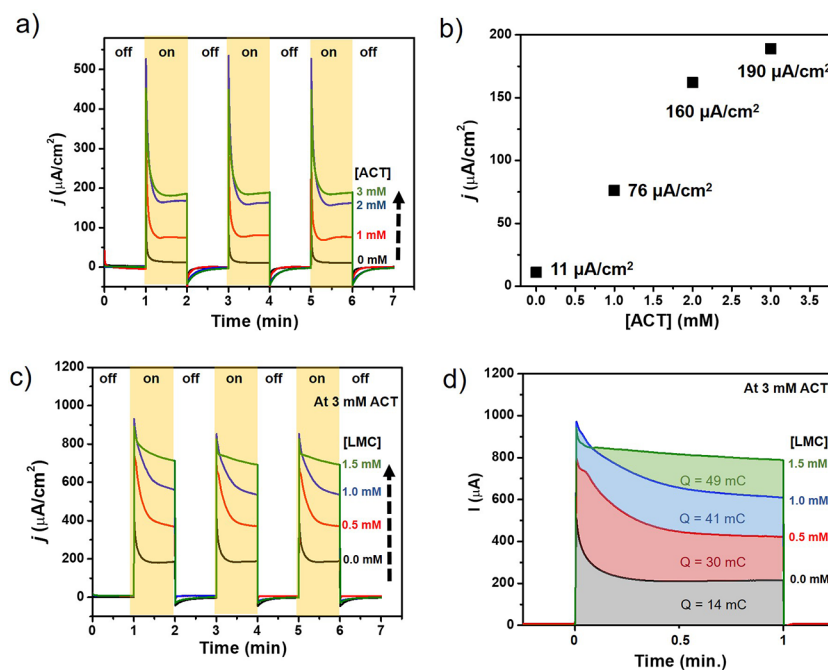


Figure 4. (a) Photocurrent–time traces measured with the FTO/TiO₂ NRAs/RuC electrode (black), with 1 mM (red), 2 mM (blue), and 3 mM (green) ACT in 0.1 M tetrabutylammonium hexafluorophosphate (TBAPF₆) acetonitrile solution with an applied bias of 0.1 V vs Ag/Ag⁺ under illumination (AM 1.5G, 1 sun, 100 mW cm⁻²) with 1 min on/off cycles. (b) Plot of photocurrent vs [ACT]. (c) Photocurrent–time traces of FTO/TiO₂ NRAs/RuC electrodes with 3 mM ACT and increasing LMC concentrations from 0 to 1.5 mM (0.5 mM increments). (d) Chronoamperograms of the FTO/TiO₂ NRAs/RuC electrode with 3 mM ACT in the presence of LMC from 0 to 1 min. The FTO/TiO₂ NRAs/RuC active cell area was 1.14 cm² for measurements of photocurrent–time traces.

than 0.3 V vs Ag/Ag⁺ will cause substantial background current. The addition of LMC with ACT in solution (blue voltammogram in Figure 3b) introduces a catalytic wave coinciding with the formation of the oxoammonium species. The blue voltammogram does not reach a diffusion-controlled steady state due to the catalytic regeneration of reduced N-oxyl (R₂NO• or N-hydroxyl R₂NOH) after reaction with LMC and subsequent reformation of the oxoammonium ACT⁺ at the electrode surface. The FTO/TiO₂ NRAs/RuC surface in the presence of just LMC in solution only shows increased anodic currents at a higher applied bias (Figure S5) highlighting the importance of ACT as a hydrogen atom transfer mediator to activate the oxidation of LMC. While carried out under dark conditions, these results show that (1) RuC^{III} is electrochemically competent to form the active oxoammonium ACT⁺ species, and (2) the direct electrochemical activation of this process occurs only at higher applied bias, namely, above 0.4 V vs Ag/Ag⁺. An increase in the current at more negative applied bias under illumination with visible light then indicates effective photochemical activation of the system.

The photochemical behavior of the HAT-DSPEC photoanode in the presence of the nitroxyl radical ACT and ACT plus the phenolic lignin model compound LMC is shown in Figure 4. The photocurrent response of the FTO/TiO₂ NRAs/RuC electrode in a nonaqueous electrolyte was examined with increasing ACT concentration during light on/off cycles under AM 1.5G illumination (100 mW cm⁻²), with an applied bias 0.1 V vs Ag/Ag⁺. As shown in Figure 4a, the FTO/TiO₂ NRAs/RuC with ACT showed a significant increase in maximum photocurrent up to approximately 190 $\mu\text{A}/\text{cm}^2$. This aminoxyl radical (or the corresponding hydroxylamine) from ACT can serve as a source of electrons, regenerating the ground-state Ru(II) photocatalyst following charge injection of RuC^{II*} to

TiO₂ and subsequent formation of Ru(III) as the first electron transfer step in the process.⁴³ Increasing [ACT] from 0 to 2 mM results in a pronounced increase linearly from ~11 to 160 $\mu\text{A}/\text{cm}^2$, and then the addition of 3 mM ACT reaches a saturation level of photocurrent 190 $\mu\text{A}/\text{cm}^2$ shown in Figure 4b. Next, the photocurrent transients were measured in the presence of LMC under the same photochemical conditions used for the photocurrents with [ACT] = 3 mM in Figure 4c. The addition of LMC (from 0 to 1.5 mM) to solution leads to a remarkable increase in the photocurrent from ~190 to 690 $\mu\text{A}/\text{cm}^2$ measured at the FTO/TiO₂ NRAs/RuC photoanode. The integration of the resulting time/photocurrent traces gives the total charge passed during the photocurrent measurements. The photocurrent transients at the FTO/TiO₂ NRAs/RuC photoanode coupled with 3 mM ACT revealed the total consumed charges of 14, 30, 41, and 49 mC for 0.0, 0.5, 1.0, and 1.5 mM LMC, respectively (Figure 4d). Compared to the absence of LMC, this total consumed charge increased by approximately 250% in the presence of LMC (1.5 mM), is attributed to effective LMC oxidation in the redox reactions, and provides the basis of a high photocatalytic turnover number (PTON) observed in this HAT-DSPEC system. This observation in the presence of LMC supports the emission quenching experiment, in which the addition of LMC showed the highly efficient quenching with RuC/ACT. We assume that LMC plays an important role of a sacrificial mediator in an HAT-DSPEC system. Sequentially, this behavior is believed to proceed by (1) light absorption and e⁻ injection from RuC to the TiO₂ NRA surface, (2) oxidation of ACT to form ACT⁺ by RuC(III) reforming the ground-state RuC(II), and (3) HAT oxidation of LMC by ACT⁺ regenerating the hydroxylamine radical R₂NO• (or the reduced aminoxyl radical R₂NOH).

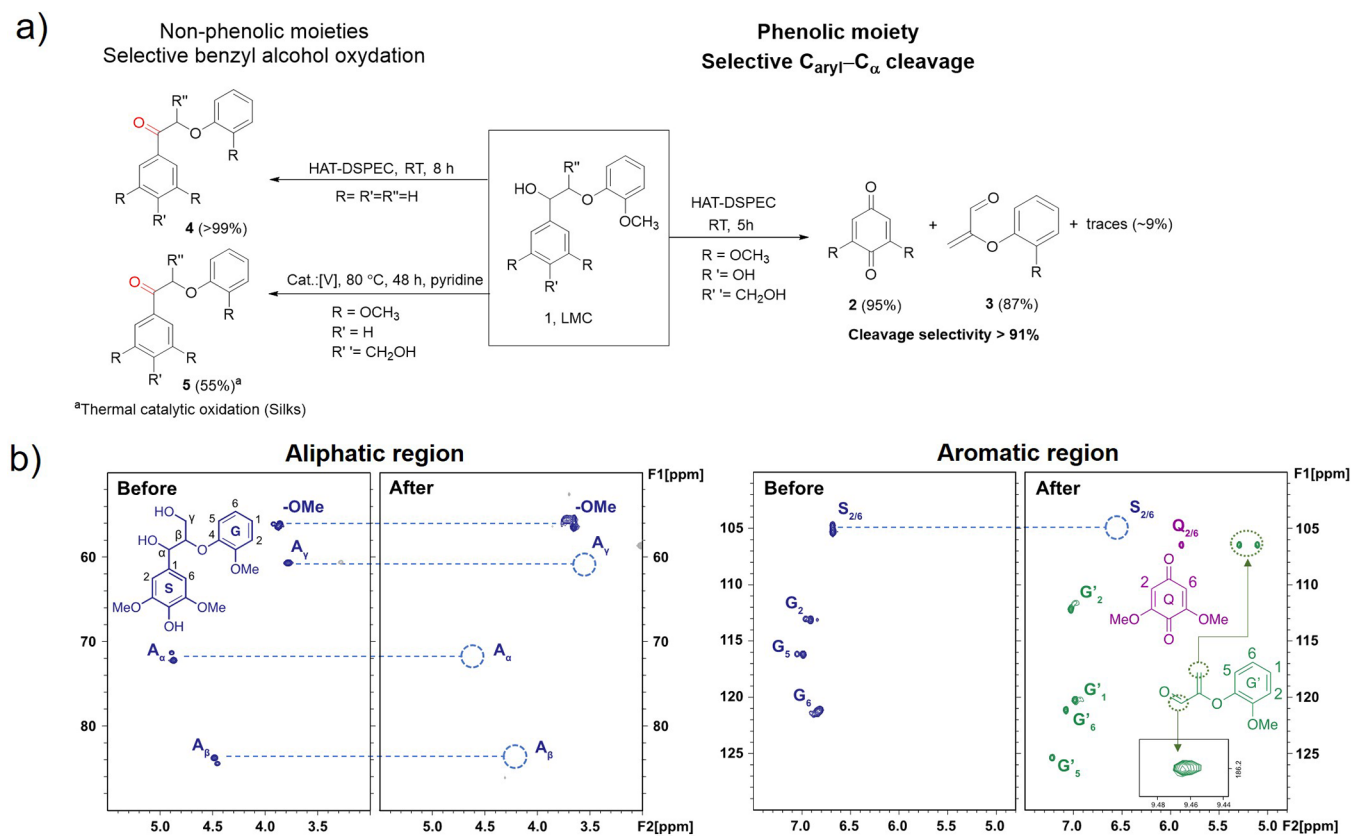


Figure 5. (a) Photocatalytic C–C bond cleavage reaction of a phenolic lignin model compound **LMC** in an HAT-DSPEC at room temperature (right). Yields and selectivity were determined by ^1H NMR analysis of the crude reaction mixtures relative to dimethyl sulfoxide (DMSO) internal standard. Selective 2° benzyl alcohol oxydation of nonphenolic compounds using a heterogeneous HAT-DSPEC and thermal catalytic method (left). (footnote a) The published value, 55%, from ref 17 was used for the product yield of the nonphenolic lignin model compound **5**. (b) Aliphatic and aromatic regions of 2D HSQC NMR spectra of the **LMC** before and after photocatalytic reactions under the standard conditions in the HAT-DSPEC.

The above experiments give a strong indication that an HAT-DSPEC can serve as a heterogeneous photocatalytic system under mild aerobic conditions for the selective C–C bond cleavage of **LMC** which structurally mimics the abundant phenolic groups present in lignin.⁴⁴ To perform the photocatalytic conversion of **LMC** in an HAT-DSPEC, **LMC** (15.0 mg, 0.044 mmol) and **ACT** (6.0 mg, 0.028 mmol) were dissolved in 5.0 mL of acetonitrile containing TBAPF₆ (0.2 g, 0.5 mmol). A 5 h continuous illumination experiment was performed with the photoanode active cell area $\sim 2.1\text{ cm}^2$ under an applied bias of 0.1 V vs Ag/Ag⁺ with an AM1.5G (100 mW cm⁻²) solar simulator using the aforementioned conditions. By examination of ^1H and ^{13}C NMR, **LMC** was completely consumed, and cleavage products **2** and **3** were observed after 5 h at room temperature (Figure S6). The oxidative reaction in an HAT-DSPEC afforded the chemoselective C_{aryl}–C_α bond cleavage products **2** (95%) and 2,6-dimethoxybenzoquinone **3** (87%) (Figure 5a). The yield was determined by ^1H NMR with DMSO as an internal standard. Previously, we investigated the selective oxidation of the secondary alcohol C_α–OH to ketone C_α=O in the nonphenolic group of the lignin model compound in a DSPEC with NHPI/2,6-lutidine as an HAT cocatalyst.⁸ On the basis of our previous study, the oxidation of the secondary alcohol results in the disappearance of H_α and a new chemical shift due to the conversion of C_α–OH to C_α=O in the β-O-4 aryl ether linkages. Very interestingly, the two-dimensional

^1H – ^{13}C heteronuclear single quantum coherence (2D HSQC NMR) spectra of the starting **LMC** (H_α at δ_{H} 4.72 and δ_{C} 72.34 ppm, H_β peaks at δ_{H} 4.33 and δ_{C} 84.06 ppm in the aliphatic region) completely disappeared following the illumination period (Figure 5b, left). This disappearance can be attributed to C–C and/or C–O bond cleavages in **LMC**. Moreover, 2D HSQC NMR signals were observed for new chemical shifts, δ_{H} 9.47 and δ_{C} 186.18 ppm (Figure 5b, right, inset), suggesting the formation of aldehyde-containing monomeric products from **LMC**. In the aromatic region, the characteristic signals of **2** and **3** are attributed to C–C bond scission.

To gain more insight into the influence of the **RuC** photocatalyst and the need for applied illumination to support the conversion of **LMC** to **2** and **3**, several control experiments with product analysis by 2D HSQC NMR spectroscopy were performed as shown in Figure S7. In these experiments, it was observed that only $\sim 10\%$ of the secondary alcohol C_α–OH converted to the ketone C_α=O without light illumination or **RuC** present. The observation of a slight production of the ketone indicates that electrocatalytic oxidation of the 2° benzyl alcohol C_α–OH might occur due to the applied bias of 0.1 V vs Ag/Ag⁺ used in the photochemical experiments and the presence of **LMC**. It is interesting to note that the current of FTO/TiO₂ NRAs with **ACT** and **LMC** is increased to 12 μA compared to that of FTO/TiO₂ NRAs with **ACT** without **LMC** in Figure S5. **LMC** can be a sacrificial mediator and/or

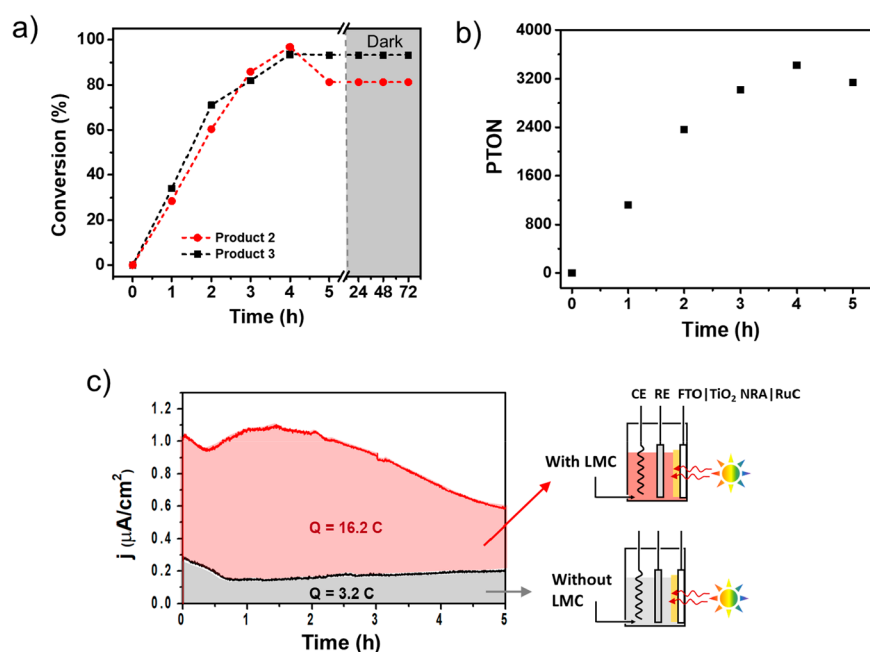


Figure 6. (a) Conversion of LMC to major products 2 and 3 monitored by GC-FID with and without 1 sun light illumination over 72 h. (b) PTON plot as a function of time. (c) Long-term photocurrent density of an HAT-DSPEC with (red shade) and without (gray shade) LMC in 0.1 M TBAPF₆ with 3 mM HAT under an applied bias of 0.1 V vs Ag/Ag⁺ at ambient temperature in an aerobic condition. The active photoanode was irradiated by an AM 1.5G solar simulator (1 sun, 100 mW cm⁻²). Illustration (right) comparing the HAT-DSPEC with and without LMC using a three-electrode cell [working electrode (WE), FTO|TiO₂ NRAs|RuC; counter electrode (CE), Pt; reference electrode (RE), nonaqueous Ag/Ag⁺].

oxidizing agent leading to oxidation of the secondary alcohol C_α—OH despite being under a low bias, 0.1 V vs Ag/Ag⁺. These control experiments prove that the presence of RuC and light is essential, and any electrochemical oxidation does not result in bond cleavage as the H_α and H_β peaks in the aliphatic region remain after the illumination period in the control. Taken together, the examination of photocatalytic LMC in the HAT-DSPEC system under 1 sun illumination at room temperature revealed the evidence for cleavage of the C—C bond of aryl ether β-O-4 linkages in LMC. We hypothesized that the pendant 4-phenolic group in LMC may contribute to the unusual photocatalytic cleavage observed of the aryl C_{aryl}—C_α bond. According to the literature, the catalytic oxidative reactions of the nonphenolic lignin model compound (5, R = OCH₃, R' = H, R'' = CH₂OH) and phenolic lignin model compound (LMC, R = OCH₃, R' = OH, R'' = CH₂OH) were tested with a vanadium catalyst in the presence of pyridine at 80 °C for 48 h (Figure 5a).³⁰ To confirm this, a nonphenolic lignin model compound, 2-phenoxy-1-phenylethanol (PP-ol, R = R' = R'' = H), was tested under the same photochemical conditions used for LMC (Figure 5a). Interestingly, no oxidative cleavage of the C—C bond in the β-O-4 aryl ether linkage was observed though oxidative conversion of secondary benzylic alcohol, C_α—OH, to the ketone form C_α=O (4) occurred within 8.5 h at ambient temperature as monitored by a flame ionization detector in gas chromatography (GC-FID) (Figure S8). We conclude that the presence of a phenoxy group in the lignin model compound is essential for the C—C bond cleavage.

In order to investigate the irreversible LMC oxidative cleavage reaction more directly, the LMC oxidized species present in solution was characterized by a GC-FID. The selective cleavage products of 2 and 3 were monitored by comparing the chromatogram peak intensities with the

retention times of 14.92 min for 2 and 12.59 min for 3 (Figure S9). DMSO was injected into the mixture solution as an internal standard. The data show that direct cleavage of the C—C bond was >95% after the 4 h experiment (Figure 6a). Interestingly, while product 3 was kept as 93% yield after the 5 h continuous illumination, the product yield of 2 decreased slightly after 4 h. We assumed that the monomeric benzoquinone 2 can be further oxidized to a dimeric benzoquinone by the strong oxidized mediate HAT⁺ without the light illumination. However, a 5 to 72 h dark period after illumination resulted in no net change in the amount of product 2 and 3 formed in an HAT-DSPEC system, thus indicating that the reaction selectivity was dependent on the reaction time and the presence of illumination.

According to the above experiments, the RuC photocatalyst adsorbed to the TiO₂ NRAs plays an important role of photon absorption and activates the HAT to catalyze the oxidative cleavage reaction. The photocatalytic activity of RuC, PTON, which represents the effectiveness of the photocatalyst in this reaction system, was evaluated by GC-FID. The number of moles of selective bond cleavage products of 2 and 3 from LMC was determined and quantified by GC-FID over 5 h. PTONs at various points during the 5 h illumination experiment were determined by dividing the average mol amount of 2 and 3 measured by the mol amount of RuC adsorbed to the electrode surface. This gave PTON values of 1120, 2360, 3020, 3420, and 3140 for time points of 1, 2, 3, 4, and 5 h, respectively (Figure 6b). These results suggested that the HAT-DSPEC system incorporating the heterogeneous photocatalyst RuC yields an excellent PTON for the oxidative C_{aryl}—C_α bond cleavage reaction in the phenolic LMC. Furthermore, the sustained photocurrent of the complete photoanode was monitored in the absence and presence of LMC during 5 h of continuous illumination (Figure 6c). The

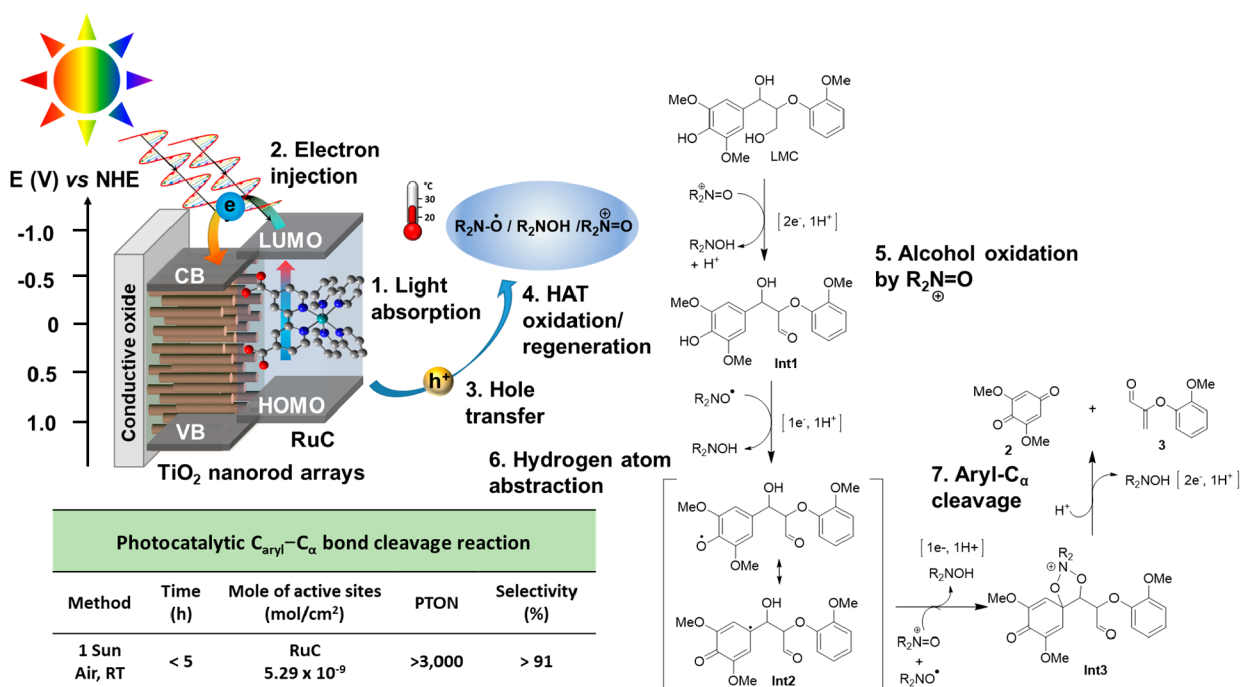
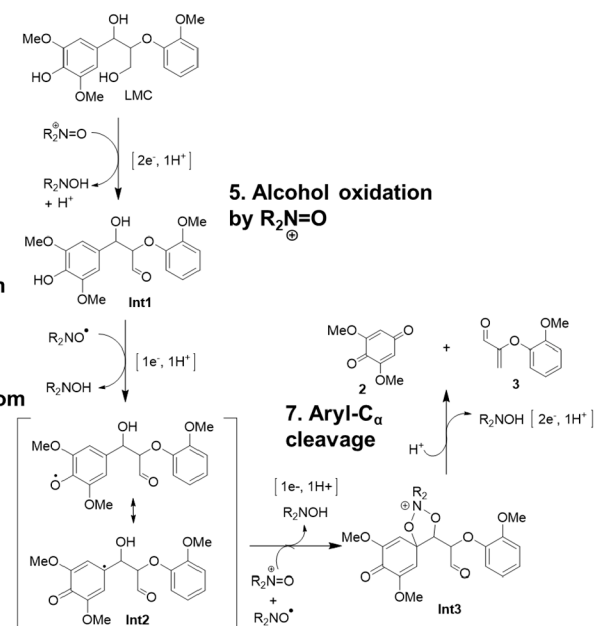


Figure 7. Proposed mechanism for C_{aryl}-C_α bond cleavage of LMC by the HAT-DSPEC.

anodic current gradually decreased over the prolonged illumination time, which is in part attributed to the irreversible consumption of LMC and/or degradation of RuC on the TiO₂ NRA surface during the experiment period.^{20,21,28}

As shown in Figure 7, the above measurements reveal a possible reaction mechanism for the oxidative C_{aryl}-C_α bond cleavage following a series of photodynamic events: after photoexcitation of the surface-bound photocatalyst RuC on the FTO/TiO₂ NRAs (step 1), the excited-state RuC* is formed. Electron and hole generation (TiO₂ NRAs (e⁻) and RuC(III), respectively) occurs following electron injection into the conduction band of TiO₂ NRAs (step 2). Upon the hole transfer from Ru(III) to ACT (R₂N-O•) mediator in solution, the ground-state RuC(II) regenerates (step 3). Oxidation of R₂N-O• after hole transfer generates the oxoammonium R₂N⁺=O (ACT⁺), which is a strong oxidizing agent and the active species for alcohol oxidation of LMC (step 4). The photochemical formation of ACT⁺, and the buildup of a pool of ACT⁺ near the photoanode surface, then initiates a series of steps which ultimately lead to the formation of 2 and 3. Given the structure of each product 2 and 3 as determined by ¹H and ¹³C NMR, GC-FID, and 2D HSQC NMR and a comparison with model compounds of each, the overall conversion represents a 6 e⁻, 4 H⁺ oxidation of LMC. The exact mechanistic details are the focus of ongoing study, and elucidation of the mechanism is outside the scope of the current work; however, we hypothesize the consumption of 2 equiv of ACT⁺ and 2 equiv of ACT in the formation of 2 and 3 yielding 4 equiv of R₂N-OH (ACTOH). One equiv of the oxoammonium likely oxidizes the γ-hydroxyl group in LMC (the less sterically hindered primary alcohol), resulting in the formation of Int1 (step 5).^{20,45} The phenoxy radical species (in Int2) in the para position might form following hydrogen atom abstraction by the R₂N-O•, and the resulting semiquinone intermediate is imperative to observe the products of C-C bond cleavage (step 6). Model compounds that do not contain the para-hydroxyl group do not undergo



cleavage, and this leads us to infer the importance of the radical resonance form in Int2. The consumption of an additional 1 equiv of ACT⁺ and 1 equiv of ACT possibly proceeds through the pentacyclic intermediate Int3 (step 7). Mechanistic studies are planned and currently underway to explore the details of the C-C bond cleavage observed and will be the focus of future reports.

Recently, Meyer, Schanze, and co-workers reported the use of a mesoporous structured TiO₂ (nanoTiO₂) type DSPEC system containing Ru(II)-based chromophore-water oxidation catalyst assemblies for light-driven photochemical oxidation.^{24-26,46,47} For example, light-driven phenol (PhOH) and benzyl alcohol (BnOH) oxidation experiments were carried out in a nanoTiO₂ type DSPEC under 1 sun illumination.³³ With the similar surface coverage of photocatalyst (6.90 × 10⁻⁹ mol cm⁻²) compared to that of RuC (5.29 × 10⁻⁹ mol cm⁻²) used for the current approach, the maximum photocurrents in the presence of PhOH and BnOH were observed to be 11.5 and 8.5 μA cm⁻², respectively. Recently, we tested a lignin model compound in a nanoTiO₂ type DSPEC in the presence of the NHPI/base pair under illumination (2 sun) over 20 h for light-driven benzylic alcohol oxidation.²¹ The maximum photocurrent with the surface coverage of RuC (4.5 × 10⁻⁸ mol cm⁻²) was observed around 145 μA cm⁻². Surprisingly, compared to these previous studies, the photoelectrochemical performance with the TiO₂ NRA-based HAT-DSPEC is remarkably improved for visible-light-driven oxidation reactions. The photocurrent generated from HAT-DSPEC with LMC is ~690 μA cm⁻² under 1 sun and with 5.29 × 10⁻⁹ mol cm⁻² RuC. Moreover, the present HAT-DSPEC system exhibits excellent selectivity and PTON under 1 sun illumination at room temperature during a 5 h photolysis compared to the thermocatalytic approach which only gave ~55% of product yield using a homogeneous catalyst for C-C bond cleavage at a reaction temperature of 80 °C over 48 h.³⁰ Therefore, the present work reports, for the first time, the use of a TiO₂ NRA type HAT-DSPEC under ambient conditions

to carry out the photocatalytic selective C_{aryl}–C_α bond cleavage reactions of a lignin model compound.

CONCLUSION

An HAT-DSPEC has been fabricated by incorporating a one-dimensional TiO₂ NRA type photoanode containing photocatalyst RuC with an HAT mediator. The HAT-DSPEC system is able to activate oxidative bond cleavage of a model compound based on a common motif found in lignin and demonstrates a remarkable photocurrent using 5.29 nmol cm⁻² RuC. The system yielded high PTON and excellent selectivity for C_{aryl}–C_α bond cleavage of LMC under 1 sun illumination, ambient temperature, and aerobic conditions. Further optimization of the morphology of TiO₂ NRAs and the structure of photocatalyst RuC and HAT may enable an increase in photocatalytic activity for light-driven oxidative cleavage reactions. These studies will be carried out in upcoming reports. Future work will perform solar-light-driven degradation of native lignin containing abundant phenolic groups in a one-dimensional TiO₂ NRA type HAT-DSPEC under mild conditions. This report indicates that this first approach in a one-dimensional TiO₂ NRA type HAT-DSPEC has expanded the scope of phenolic-containing biomacromolecules or petroleum-based polymer for solar-light-driven polymer degradation with selective bond cleavage under mild conditions.

ASSOCIATED CONTENT

Supporting Information

The Supporting Information is available free of charge at <https://pubs.acs.org/doi/10.1021/acscatal.1c00198>.

Details of materials, characterization methods, and characterization data (PDF)

AUTHOR INFORMATION

Corresponding Author

Gyu Leem – Department of Chemistry, State University of New York College of Environmental Science and Forestry, Syracuse, New York 13210, United States; The Michael M. Szwarc Polymer Research Institute, Syracuse, New York 13210, United States; orcid.org/0000-0003-0169-1096; Email: gyleem@esf.edu

Authors

Shuya Li – Department of Chemistry, State University of New York College of Environmental Science and Forestry, Syracuse, New York 13210, United States

Saerona Kim – Department of Chemistry, State University of New York College of Environmental Science and Forestry, Syracuse, New York 13210, United States

Andrew H. Davis – Department of Chemistry, Syracuse University, Syracuse, New York 13244, United States

Jingshun Zhuang – Department of Chemical Engineering, State University of New York College of Environmental Science and Forestry, Syracuse, New York 13210, United States

Eric Wolfgang Shuler – Department of Chemistry, State University of New York College of Environmental Science and Forestry, Syracuse, New York 13210, United States

Debora Willinger – Department of Chemistry and Biochemistry, College of Science and Engineering, Texas

Christian University, Fort Worth, Texas 76129, United States

Jae-Joon Lee – Department of Energy Materials and Engineering, Research Center for Photoenergy Harvesting & Conversion Technology (phct), Dongguk University, Seoul 04620, Republic of Korea; orcid.org/0000-0001-8966-0336

Weiwei Zheng – Department of Chemistry, Syracuse University, Syracuse, New York 13244, United States; orcid.org/0000-0003-1394-1806

Benjamin D. Sherman – Department of Chemistry and Biochemistry, College of Science and Engineering, Texas Christian University, Fort Worth, Texas 76129, United States; orcid.org/0000-0001-9571-5065

Chang Geun Yoo – Department of Chemical Engineering, State University of New York College of Environmental Science and Forestry, Syracuse, New York 13210, United States

Complete contact information is available at: <https://pubs.acs.org/10.1021/acscatal.1c00198>

Author Contributions

S.L. conceived the project with G.L. providing overall supervision. S.K., A.H.D., J.Z., E.W.S., and D.W. contributed to data acquisition and analysis. J.-J.L., W.Z., B.D.S., and C.G.Y. added conceptual contributions and edited the manuscript. All authors contributed to the discussion of the results presented and editing.

Notes

The authors declare no competing financial interest.

ACKNOWLEDGMENTS

Financial support from State University of New York, College of Environmental Science and Forestry (SUNY ESF) is gratefully acknowledged. W.Z. acknowledges support from ACS Petroleum Research Fund under Award 59861-DNIS and NSF CAREER under Award CHE-1944978. J.-J.L. acknowledge the financial support from the Ministry of Science, ICT & Future Planning (NRF-2016M1A2A2940912). We also thank Alexander B. Artyukhin and David Kiemle in the Analytical & Q Technical Services (A&TS) at SUNY ESF for help with GC. D.W. thanks the TCU College of Science and Engineering for financial support of this work through a SERC graduate research grant. B.D.S. acknowledges start-up funding from Texas Christian University for support of this work.

REFERENCES

- (1) Shuai, L.; Sitison, J.; Sadula, S.; Ding, J.; Thies, M. C.; Saha, B. Selective C-C Bond Cleavage of Methylene-Linked Lignin Models and Kraft Lignin. *ACS Catal.* **2018**, *8*, 6507–6512.
- (2) McDonald, T. R.; Mills, L. R.; West, M. S.; Rousseaux, S. A. L. Selective Carbon-Carbon Bond Cleavage of Cyclopropanols. *Chem. Rev.* **2021**, *121*, 3–79.
- (3) Yu, X.-Y.; Chen, J.-R.; Xiao, W.-J. Visible Light-Driven Radical-Mediated C-C Bond Cleavage/Functionalization in Organic Synthesis. *Chem. Rev.* **2021**, *121*, 506–561.
- (4) Wang, Y.; Wang, Q.; He, J.; Zhang, Y. Highly Effective C-C Bond Cleavage of Lignin Model Compounds. *Green Chem.* **2017**, *19*, 3135–3141.
- (5) Ma, Y.; Du, Z.; Liu, J.; Xia, F.; Xu, J. Selective Oxidative C-C Bond Cleavage of a Lignin Model Compound in the Presence of Acetic Acid with a Vanadium Catalyst. *Green Chem.* **2015**, *17*, 4968–4973.

- (6) Liu, H.; Li, H.; Lu, J.; Zeng, S.; Wang, M.; Luo, N.; Xu, S.; Wang, F. Photocatalytic Cleavage of C-C Bond in Lignin Models under Visible Light on Mesoporous Graphitic Carbon Nitride through π - π Stacking Interaction. *ACS Catal.* **2018**, *8*, 4761–4771.
- (7) Rahimi, A.; Ulbrich, A.; Coon, J. J.; Stahl, S. S. Formic-Acid-Induced Depolymerization of Oxidized Lignin to Aromatics. *Nature* **2014**, *515*, 249–252.
- (8) Wi, S. G.; Cho, E. J.; Lee, D.-S.; Lee, S. J.; Lee, Y. J.; Bae, H.-J. Lignocellulose Conversion for Biofuel: A New Pretreatment Greatly Improves Downstream Biocatalytic Hydrolysis of Various Lignocellulosic Materials. *Biotechnol. Biofuels* **2015**, *8*, 228.
- (9) Xu, Z.; Lei, P.; Zhai, R.; Wen, Z.; Jin, M. Recent Advances in Lignin Valorization with Bacterial Cultures: Microorganisms, Metabolic Pathways, and Bio-Products. *Biotechnol. Biofuels* **2019**, *12*, 32.
- (10) Abdullah, B.; Muhammad, S. A. F. A. S.; Mahmood, N. A. N. Production of Biofuel via Hydrogenation of Lignin from Biomass. In *New Advances in Hydrogenation Processes—Fundamentals and Applications*; IntechOpen, 2017. DOI: 10.5772/66108.
- (11) Chakar, F. S.; Ragauskas, A. J. Review of Current and Future Softwood Kraft Lignin Process Chemistry. *Ind. Crops Prod.* **2004**, *20*, 131–141.
- (12) Srivastava, S. K.; Singh, A. K.; Sharma, A. Studies on the Uptake of Lead and Zinc by Lignin Obtained from Black Liquor - a Paper Industry Waste Material. *Environ. Technol.* **1994**, *15*, 353–361.
- (13) Calvo-Flores, F. G.; Dobado, J. A. Lignin as Renewable Raw Material. *ChemSusChem* **2010**, *3*, 1227–1235.
- (14) Nguyen, S. T.; Murray, P. R. D.; Knowles, R. R. Light-Driven Depolymerization of Native Lignin Enabled by Proton-Coupled Electron Transfer. *ACS Catal.* **2020**, *10*, 800–805.
- (15) Wu, X.; Fan, X.; Xie, S.; Lin, J.; Cheng, J.; Zhang, Q.; Chen, L.; Wang, Y. Solar Energy-Driven Lignin-First Approach to Full Utilization of Lignocellulosic Biomass under Mild Conditions. *Nat. Catal.* **2018**, *1*, 772–780.
- (16) Nguyen, J. D.; Matsuura, B. S.; Stephenson, C. R. J. A Photochemical Strategy for Lignin Degradation at Room Temperature. *J. Am. Chem. Soc.* **2014**, *136*, 1218–1221.
- (17) Gazi, S.; Ng, W. K. H.; Ganguly, R.; Moeljadi, A. M. P.; Hira, H.; Soo, H. S. Selective Photocatalytic C-C Bond Cleavage under Ambient Conditions with Earth Abundant Vanadium Complexes. *Chem. Sci.* **2015**, *6*, 7130–7142.
- (18) Bosque, I.; Magallanes, G.; Rigoulet, M.; Kärkäs, M. D.; Stephenson, C. R. J. Redox Catalysis Facilitates Lignin Depolymerization. *ACS Cent. Sci.* **2017**, *3*, 621–628.
- (19) Wang, F.; Stahl, S. S. Electrochemical Oxidation of Organic Molecules at Lower Overpotential: Accessing Broader Functional Group Compatibility with Electron-Proton Transfer Mediators. *Acc. Chem. Res.* **2020**, *53*, 561–574.
- (20) Rafiee, M.; Alherech, M.; Karlen, S. D.; Stahl, S. S. Electrochemical Aminoxyl-Mediated Oxidation of Primary Alcohols in Lignin to Carboxylic Acids: Polymer Modification and Depolymerization. *J. Am. Chem. Soc.* **2019**, *141*, 15266–15276.
- (21) Li, S.; Li, Z.-J.; Yu, H.; Sytu, M. R.; Wang, Y.; Beeri, D.; Zheng, W.; Sherman, B. D.; Yoo, C. G.; Leem, G. Solar-Driven Lignin Oxidation via Hydrogen Atom Transfer with a Dye-Sensitized TiO₂ Photoanode. *ACS Energy Lett.* **2020**, *5*, 777–784.
- (22) Sherman, B. D.; Xie, Y.; Sheridan, M. V.; Wang, D.; Shaffer, D. W.; Meyer, T. J.; Concepcion, J. J. Light-Driven Water Splitting by a Covalently Linked Ruthenium-Based Chromophore-Catalyst Assembly. *ACS Energy Lett.* **2017**, *2*, 124–128.
- (23) Badgurjar, D.; Shan, B.; Nayak, A.; Wu, L.; Chitta, R.; Meyer, T. J. Electron-Withdrawing Boron Dipyrromethene Dyes as Visible Light Absorber/Sensitizers on Semiconductor Oxide Surfaces. *ACS Appl. Mater. Interfaces* **2020**, *12*, 7768–7776.
- (24) Sherman, B. D.; Sheridan, M. V.; Wee, K.-R.; Marquard, S. L.; Wang, D.; Alibabaei, L.; Ashford, D. L.; Meyer, T. J. A Dye-Sensitized Photoelectrochemical Tandem Cell for Light Driven Hydrogen Production from Water. *J. Am. Chem. Soc.* **2016**, *138*, 16745–16753.
- (25) Leem, G.; Sherman, B. D.; Burnett, A. J.; Morseth, Z. A.; Wee, K.-R.; Papanikolas, J. M.; Meyer, T. J.; Schanze, K. S. Light-Driven Water Oxidation Using Polyelectrolyte Layer-by-Layer Chromophore-Catalyst Assemblies. *ACS Energy Lett.* **2016**, *1*, 339–343.
- (26) Leem, G.; Morseth, Z. A.; Puodziukynaitė, E.; Jiang, J.; Fang, Z.; Gilligan, A. T.; Reynolds, J. R.; Papanikolas, J. M.; Schanze, K. S. Light Harvesting and Charge Separation in a π -Conjugated Antenna Polymer Bound to TiO₂. *J. Phys. Chem. C* **2014**, *118*, 28535–28541.
- (27) Leem, G.; Black, H. T.; Shan, B.; Bantang, J. P. O.; Meyer, T. J.; Reynolds, J. R.; Schanze, K. S. Photocathode Chromophore-Catalyst Assembly via Layer-By-Layer Deposition of a Low Band-Gap Isoindigo Conjugated Polyelectrolyte. *ACS Appl. Energy Mater.* **2018**, *1*, 62–67.
- (28) Hyde, J. T.; Hanson, K.; Vannucci, A. K.; Lapidés, A. M.; Alibabaei, L.; Norris, M. R.; Meyer, T. J.; Harrison, D. P. Electrochemical Instability of Phosphonate-Derivatized, Ruthenium(III) Polypyridyl Complexes on Metal Oxide Surfaces. *ACS Appl. Mater. Interfaces* **2015**, *7*, 9554–9562.
- (29) Du, X.; Zhang, H.; Sullivan, K. P.; Gogoi, P.; Deng, Y. Electrochemical Lignin Conversion. *ChemSusChem* **2020**, *13*, 4318–4343.
- (30) Hanson, S. K.; Wu, R.; Silks, L. A. Pete. C-C or C-O Bond Cleavage in a Phenolic Lignin Model Compound: Selectivity Depends on Vanadium Catalyst. *Angew. Chem., Int. Ed.* **2012**, *51*, 3410–3413.
- (31) Jiang, Y.-Y.; Yan, L.; Yu, H.-Z.; Zhang, Q.; Fu, Y. Mechanism of Vanadium-Catalyzed Selective C-O and C-C Cleavage of Lignin Model Compound. *ACS Catal.* **2016**, *6*, 4399–4410.
- (32) Grätzel, M. Recent Advances in Sensitized Mesoscopic Solar Cells. *Acc. Chem. Res.* **2009**, *42*, 1788–1798.
- (33) Huang, C.; Bian, J.; Zhang, R.-Q. Role of Cl Ion Desorption in Photocurrent Enhancement of the Annealed Rutile Single-Crystalline TiO₂ Nanorod Arrays. *J. Phys. Chem. C* **2017**, *121*, 18892–18899.
- (34) El-Shafei, A.; Hussain, M.; Islam, A.; Han, L. Structure-Property Relationship of Hetero-Aromatic-Electron-Donor Antennas of Polypyridyl Ru(II) Complexes for High Efficiency Dye-Sensitized Solar Cells. *Prog. Photovoltaics* **2014**, *22*, 958–969.
- (35) Eberhart, M. S.; Bowers, L. M. R.; Shan, B.; Troian-Gautier, L.; Brennaman, M. K.; Papanikolas, J. M.; Meyer, T. J. Completing a Charge Transport Chain for Artificial Photosynthesis. *J. Am. Chem. Soc.* **2018**, *140*, 9823–9826.
- (36) Brennaman, M. K.; Dillon, R. J.; Alibabaei, L.; Gish, M. K.; Dares, C. J.; Ashford, D. L.; House, R. L.; Meyer, G. J.; Papanikolas, J. M.; Meyer, T. J. Finding the Way to Solar Fuels with Dye-Sensitized Photoelectrosynthesis Cells. *J. Am. Chem. Soc.* **2016**, *138*, 13085–13102.
- (37) Leem, G.; Sherman, B. D.; Schanze, K. S. Polymer-Based Chromophore-Catalyst Assemblies for Solar Energy Conversion. *Nano Converg.* **2017**, *4*, 37.
- (38) Poynton, F. E.; Bright, S. A.; Blasco, S.; Williams, D. C.; Kelly, J. M.; Gunnlaugsson, T. The Development of Ruthenium(II) Polypyridyl Complexes and Conjugates for in Vitro Cellular and in Vivo Applications. *Chem. Soc. Rev.* **2017**, *46*, 7706–7756.
- (39) Sun, B.; Chen, Y.; Tao, L.; Zhao, H.; Zhou, G.; Xia, Y.; Wang, H.; Zhao, Y. Nanorod Array of SnO₂ Quantum Dot Interspersed Multiphase TiO₂ Heterojunctions with Highly Photocatalytic Water Splitting and Self-Rechargeable Battery-Like Applications. *ACS Appl. Mater. Interfaces* **2019**, *11*, 2071–2081.
- (40) Chen, Y.-L.; Chen, Y.-H.; Chen, J.-W.; Cao, F.; Li, L.; Luo, Z.-M.; Leu, I.-C.; Pu, Y.-C. New Insights into the Electron-Collection Efficiency Improvement of CdS-Sensitized TiO₂ Nanorod Photoelectrodes by Interfacial Seed-Layer Mediation. *ACS Appl. Mater. Interfaces* **2019**, *11*, 8126–8137.
- (41) Leem, G.; Morseth, Z. A.; Wee, K.-R.; Jiang, J.; Brennaman, M. K.; Papanikolas, J. M.; Schanze, K. S. Polymer-Based Ruthenium(II) Polypyridyl Chromophores on TiO₂ for Solar Energy Conversion. *Chem. - Asian J.* **2016**, *11*, 1257–1267.
- (42) Pan, Z.; Leem, G.; Cekli, S.; Schanze, K. S. Conjugated Polyelectrolyte-Sensitized TiO₂ Solar Cells: Effects of Chain Length

and Aggregation on Efficiency. *ACS Appl. Mater. Interfaces* **2015**, *7*, 16601–16608.

(43) Song, W.; Glasson, C. R. K.; Luo, H.; Hanson, K.; Brennaman, M. K.; Concepcion, J. J.; Meyer, T. J. Photoinduced Stepwise Oxidative Activation of a Chromophore-Catalyst Assembly on TiO₂. *J. Phys. Chem. Lett.* **2011**, *2*, 1808–1813.

(44) Tuor, U.; Wariishi, H.; Schoemaker, H. E.; Gold, M. H. Oxidation of Phenolic Arylglycerol. Beta.-Aryl Ether Lignin Model Compounds by Manganese Peroxidase from Phanerochaete Chrysosporium: Oxidative Cleavage of an. Alpha.-Carbonyl Model Compound. *Biochemistry* **1992**, *31*, 4986–4995.

(45) Patil, N. D.; Yao, S. G.; Meier, M. S.; Mobley, J. K.; Crocker, M. Selective Cleavage of the C_α-C_β Linkage in Lignin Model Compounds via Baeyer-Villiger Oxidation. *Org. Biomol. Chem.* **2015**, *13*, 3243–3254.

(46) Jiang, J.; Sherman, B. D.; Zhao, Y.; He, R.; Ghiviriga, I.; Alibabaei, L.; Meyer, T. J.; Leem, G.; Schanze, K. S. Polymer Chromophore-Catalyst Assembly for Solar Fuel Generation. *ACS Appl. Mater. Interfaces* **2017**, *9*, 19529–19534.

(47) Sherman, B. D.; Bergkamp, J. J.; Brown, C. L.; Moore, A. L.; Gust, D.; Moore, T. A. A Tandem Dye-Sensitized Photoelectrochemical Cell for Light Driven Hydrogen Production. *Energy Environ. Sci.* **2016**, *9*, 1812–1817.